

This article was downloaded by:

On: 21 January 2011

Access details: *Access Details: Free Access*

Publisher *Taylor & Francis*

Informa Ltd Registered in England and Wales Registered Number: 1072954 Registered office: Mortimer House, 37-41 Mortimer Street, London W1T 3JH, UK



The Journal of Adhesion

Publication details, including instructions for authors and subscription information:

<http://www.informaworld.com/smpp/title~content=t713453635>

Analysis of Bioadhesivity of Osteoblast Cells on Titanium Alloy Surface Modified by Nd:YAG Laser

Mohammad E. Khosroshahi^a; Javad Tavakoli^a; Mahboobeh Mahmoodi^a

^a Amirkabir University of Technology, Faculty of Biomedical Engineering, Biomaterial Group, Tehran, Iran

To cite this Article Khosroshahi, Mohammad E. , Tavakoli, Javad and Mahmoodi, Mahboobeh(2007) 'Analysis of Bioadhesivity of Osteoblast Cells on Titanium Alloy Surface Modified by Nd:YAG Laser', *The Journal of Adhesion*, 83: 2, 151 – 172

To link to this Article: DOI: 10.1080/00218460701198644

URL: <http://dx.doi.org/10.1080/00218460701198644>

PLEASE SCROLL DOWN FOR ARTICLE

Full terms and conditions of use: <http://www.informaworld.com/terms-and-conditions-of-access.pdf>

This article may be used for research, teaching and private study purposes. Any substantial or systematic reproduction, re-distribution, re-selling, loan or sub-licensing, systematic supply or distribution in any form to anyone is expressly forbidden.

The publisher does not give any warranty express or implied or make any representation that the contents will be complete or accurate or up to date. The accuracy of any instructions, formulae and drug doses should be independently verified with primary sources. The publisher shall not be liable for any loss, actions, claims, proceedings, demand or costs or damages whatsoever or howsoever caused arising directly or indirectly in connection with or arising out of the use of this material.

Analysis of Bioadhesivity of Osteoblast Cells on Titanium Alloy Surface Modified by Nd:YAG Laser

Mohammad E. Khosroshahi

Javad Tavakoli

Mahboobeh Mahmoodi

Amirkabir University of Technology, Faculty of Biomedical Engineering, Biomaterial Group, Tehran, Iran

The surface microtopography and physical–chemical results of Ti6Al4V alloy were investigated in relation to bone cell response. Nd:YAG-laser-treated surfaces with (1.06 μm wavelength, 200 μs pulse duration, and a fluence of 140 Jcm⁻² exhibited an improved hydrophilic behavior due to a lower contact angle compared with the control sample. Cell spreading on the implanted specimens was analyzed by scanning electron microscope (SEM), and their condition in a specific area was studied for 10 cells from three separate regions on the same specimen using an Image J Program software. The in vitro the in vivo tests provided some useful clinical and pathological information such as the number of adhered cells on the implant. The light microscopy assessment consisted of a complete morphological description of tissue response to the implants with different surface topography.

Keywords: Cell adhesivity; Cell spreading; Contact angle; Enzyme detachment; Nd:YAG laser; Osteoblast; Surface tension; Wettability

INTRODUCTION

Interaction of biomaterials with cells mainly depends on surface characteristics of biomaterials, including surface topography, charges, components, chemical states, and mechanical properties [1–3]. Cell adhesion is involved in various phenomena such as embryogenesis, wound healing, immune response, and metastasis as well as tissue integration of biomaterial. Thus, attachment, adhesion, and spreading

Received 30 April 2006; in final form 31 December 2006.

Address correspondence to Mohammad E. Khosroshahi, Amirkabir University of Technology, Faculty of Biomedical Engineering, Biomaterial Group, Tehran, Iran. E-mail: khosro@aut.ac.ir

will depend on the cell–material interaction and the cell’s capacity to proliferate and to differentiate itself on contact with the implant.

Titanium as a biomaterial implant has an excellent biocompatibility because it is highly inert, is not soluble in body fluids, and forms a protective oxide layer on the surface [4]. However, pure titanium could leave metal debris in the tissue because of the higher tendency to produce wear in fretting conditions. Therefore, numerous titanium alloys with improved physical and mechanical properties such as Ti6Al4V have been developed.

It is generally believed that proteins adsorbed on an implant surface can play an important role in mediating cell–surface response. Different proteins such as collagen, fibrinogen, fibronectin, and vitronectin, which act as ligands, are particularly important in osteoblast interaction with a surface. Ligands are the junctions that facilitate adhesion of bone cells to an implant surface. In other words, more ligand formation implies a better cell–surface interaction [5,6]. *In vitro* studies can be used to study the influence of surface properties on processes such as cell attachment, cell proliferation, and cell differentiation. However, *in vivo* studies must be performed to achieve a complete understanding of the healing process around implants. Previous studies have shown that the surface characteristics have a significant influence on adhesion, morphology, and maturation of cultured osteoblasts [7–10]. Also, for primary bovine osteoblasts, the wettability is one of the key factors [11]. In this study, it is shown that the wettability of the surface can provide a better spreading condition for osteoblast cells because of the reduced contact angle. It should be borne in mind that the adhesion of bone cells to an implant surface consists of two stages. In the primary stage, the cells must get close enough to the surface at an appropriate distance known as the focal distance over which the cells can easily be spread. In this respect, the wettability can provide better accessibility to the surface, thus reaching the focal distance. The secondary stage includes cell–cell attachment, which is formed by an extracellular matrix (ECM) such as fibronectin, vitronectin, etc., that acts as a protein adhesive between the cells and thus creates hydrogen bonding. However, during the past decade, laser treatment has become a promising technique for materials processing [12–15] and play an important role in improving the biocompatibility of biometals [16–18].

The aim of this research was first to produce and characterize the laser-treated Ti6Al4V alloy surface under optimum optical conditions. By that we mean that the efficiency and the quality of a material modification, in general, depends on laser parameters such as fluence, which, in turn, governs the laser energy deposition, melting, and

evaporation of titanium (in our case) during the interaction process. Thus, for performing an acceptable modification, one ought to choose a suitable section of the curve where the phase boundaries are clearly illustrated. The second goal was to carry out *in vitro* and long-term *in vivo* animal tests, and the third was to assess the adhesivity of osteoblast cells to the implant surface using an enzyme detachment test after explantation of specimens from goat bone.

MATERIALS AND METHODS

Sample Preparation

Rectangular-shaped specimens 20×10 mm and 2 mm thick were made from medical-grade Ti6Al4V (ASTM F136, Friadent, GmbH, Mannheim, Germany) with the chemical formulation Ti (91.63%), Al (5.12%), V (3.25%), by/wt.

The samples were divided into two groups of control and laser treated. All samples were cleaned with 97% ethanol and subsequently washed twice with distilled water in an ultrasonic bath (Mattachanna, Barcelona, Spain). A final rinse with deionized water at neutral pH was performed to ensure a clean surface.

Laser Setup

Surface treatment was performed by an Nd:YAG laser with 1.06- μ m wavelength, 200- μ s pulse duration, and a pulse energy of 50 J. The output beam was suitably imaged onto the target surface in a 500- μ m spot diameter where it scanned the surface at a constant velocity using a motorized XYZ translator. All the experiments were carried out in air at a pulse-repetition frequency of 1 Hz. To achieve an optimum condition for surface treatment, the melting and evaporation thresholds as well as variation of etch depth with fluence were determined by appropriate plots and scanning electron microscopy (SEM) evaluation. Material removal measurements were made by exposing the samples to a predetermined number of laser pulses (n) and measuring the depth of material removed (z_e), using a high-resolution microscope with 2- μ m depth resolution (Euromex, Prior, Cambridge, UK). The average etch rate was then calculated from z_e/n (see Figure 1).

Surface Analysis

The surface energy of the samples were determined by measuring the contact angle (θ) (Kruss-G40-instrument, Kruss, Hamburg, Germany)



FIGURE 1 Implant placement in femur bone of the goat.

of test liquids (diiodo-methane and water; Busscher, Weersals, The Netherlands) on the titanium plates and plots of the Owens–Wendt–Kaeble’s equation:

$$\gamma_{lv}(1 + \cos \theta) = 2(\gamma_l^d \cdot \gamma_s^d)^{0.5} + 2(\gamma_l^p \cdot \gamma_s^p)^{0.5} \quad (1)$$

where s and l represent solid and liquid surfaces respectively, γ^d stands for the dispersion component of the total surface energy (γ), and γ^p is the polar component.

SEM (stereoscan 360, Cambridge Instrument Company, Cambridge, England) as well as adhered cell spreading and morphology were used to examine the surface topography of the modified titanium samples.

Cell Culture

Mice connective tissue fibroblasts (L-929) with 4×10^5 ml were provided and maintained in culture medium (RPMI-1640) consisting of 100 IU/ml penicillin, 100 IU/ml streptomycin, and 10% fetal calf serum (FCS). The control sample along with two laser-treated samples ($20 \times 10 \times 2$ mm) were then placed inside the culture medium. All the samples were incubated at 37°C in 5% CO_2 atmosphere and 90% humidity for 24 h. The samples were then removed for cell growth and cytotoxicity assessment using an optical microscope (Zeiss, Göttingen, Germany).

Anesthetization

Before depilation of the operation site, the animal was completely anesthetized by injection of 2.5 mg/Kg midazolam (Dormicum[®],

Roche, Basle, Switzerland) intravenously (IV). With any sign of recovery during operation, diluted fluanisone/fentanyl (Hypnorm[®], Leeds, England) was injected slowly until an adequate effect was achieved, usually 0.2 ml at a time.

Animal Implantation

Two control and four laser-treated specimens were implanted in two legs on the upper part of the femur bone of an 8-months-old male goat weighing 30 Kg. Specimens were steam sterilized before implantation in an autoclave (Mattachnna, Barcelona, Spain). The steam sterilization was conducted under 132°C, 2 bar, and in 45 min. All the specimens were labeled by separate codes using an engraver for further studies. The operation site was shaved and depilated with soft soap and ethanol before surgery: the site was also disinfected with 70% ethanol and was covered with a sterile blanket. To proceed with implantation, the cortex bone was scraped by osteotome (Medeicon[®], Tuttlingen, Germany) after cutting the limb from the third section of the leg at the distal end near the femur and elevating it by a self-retaining retractor. Copious physiological saline solution irrigation was used during implantation to prevent overheating. To ensure a stable passive fixation of implants during the healing period, they were stabilized by size 4 and 8 titanium wires (Atila ortoped[®], Tehran, Iran) without any external compression forces (Figure 2). A light microscope (Zeiss, Gottingen, Germany) was used to examine the position of the wires after operation and no infection was observed.

After the operation the animal was protected from infection by proper prescribed uptake of penicillin for the first 4 days and gentamicine for the second 4 days. During the 8 days of recovery, multivitamins were administrated to the goat to help it regain its strength. It was held in an isolated space under room temperature, ordinary humidity, light, and air conditions, and then it was returned to its natural environment. After 8 months, the animal was sacrificed and the specimens were removed (Figure 3).

The experiments had been approved by the Yazd School of Veterinary Science (Iran) and its animal research authority and were conducted in accordance with the Animal Welfare Act of December 20, 1974, and the Regulation on Animal Experimentation of January 15, 1996. The explantation procedure was performed by first cutting the upper and lower section of femur bone using an electric saw and then the implant together with its surrounding tissues was placed in EDTA solution.



(a)



(b)

FIGURE 2 Implant removal from the femur bone of the goat: (a) before detachment of the wires and (b) the footprint of the implants on the bone.

Cell Analysis

Osteoblast cell spreading (*i.e.*, lateral growth) on the six implants (three samples for imaging and three samples for the Coulter counter) was analyzed by SEM (Stero scan 360, Cambridge, England) after removal, and their spreading condition in a specific area was studied using NIH Image J Program software (www.rsb.info.nih.gov) in three separate regions of each specimen at a frequency of 10 cells per each region. The number of attached cells in 1-cm² area of each specimen

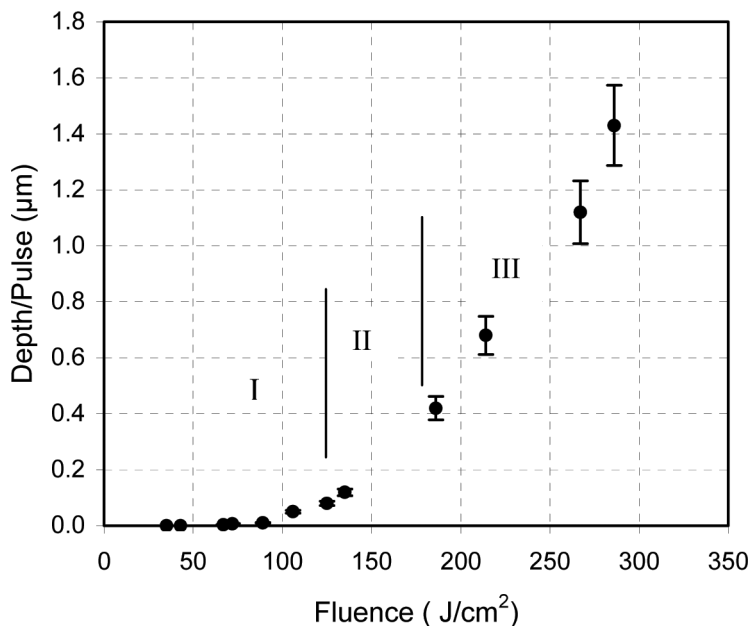


FIGURE 3 Variation of etch depth as a function of fluence.

was calculated by a Coulter counter (Eppendorf, Hamburg, Germany) using an enzyme detachment method and Trypsin-EDTA (0.025 V/V) in (PBS) phosphate buffer saline media at pH 7.5. The final amount of attached cells can be studied by plotting cell detachment rate *versus* time.

Histopathology

Following implantation, the specimens with their surrounding tissues were retrieved and prepared for histological evaluation. The specimens' related tissues were fixed in 4% formalin solution (pH 7.3), dehydrated in a graded series of ethanol (10, 30, 50, 70, and 90), and embedded in paraffin after decalcification. Then, 10-µm-thick slices were prepared per specimen using the sawing microtome technique. The slices were stained by methylene blue and basic fuchsin and studied with a light microscope (Zeiss, Gottingen, Germany). The light microscopy assessment consisted of a complete morphological description of the tissue response to the implants with different surface topography. Discriminating cell type was achieved by staining of the samples and examining related cell-shape differences. Osteoblasts can be in two states: (a) active, forming bone matrix, and (b) resting

or bone maintaining. Those make collagen, glycoproteins, and proteoglycans of bone the matrix and control the deposition of mineral crystals on the fibrils. Osteoblast becomes an osteocyte by forming a matrix around itself and is buried. Lacunae empty of osteocytes indicate dead bone. Osteoclast, a large and multinucleated cell with a pale acidophilic cytoplasm, lies on the surface of bone, often an eaten-out hollow Howship's lacuna. Macrophages are irregularly shaped cells that participate in phagocytosis.

SEM of Adhered Cells

After removal of the implants, both groups of implants were rinsed twice with phosphate buffer saline (PBS) and then fixed with 2.5% glutaraldehyde for 60 min. After a final rinse with PBS, a contrast treatment in 1% osmium tetroxide (Merck, Whitehouse Station, New Jersey, USA) was performed for 1 h, followed by an extensive rinsing in PBS and dehydration through a graded series of ethanol from 30 to 90% as described in the histology section. After free air drying, surfaces were thinly sputter coated with gold (CSD 050, with 40 mA, about 7 min).

RESULTS

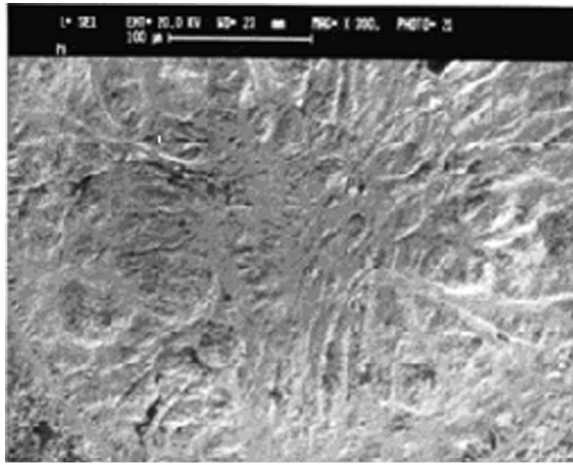
Laser Effect

Etch depth per pulse variation as a function of laser fluence (Figure 1) can be calculated from Eq. (2):

$$X = \alpha^{-1} \ln \left(\frac{F}{F_t} \right), \quad (2)$$

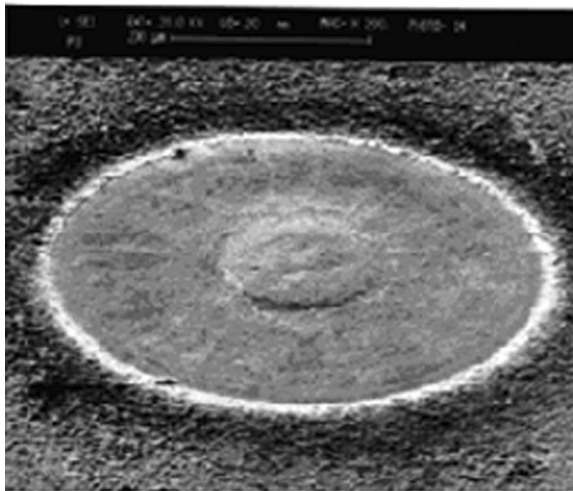
where X is etch depth, α is absorption coefficient, and F_t is threshold fluence. By using this equation, the values of α and F_t were found to be $5 \times 10^3 \text{ cm}^{-1}$ and 72 Jcm^{-2} , respectively. Interaction of laser radiation with the metal surface can be divided into three distinct regions (Figure 1).

Zone I clearly indicates that there are no morphological changes below 72 Jcm^{-2} but beyond that, where zone II commences, melting gradually occurs and continues up to 145 Jcm^{-2} . This is consistent with the fact that the power density required for melting most metals is on the order of 105 Wcm^{-2} , in our case the corresponding range would be between $365\text{--}725 \text{ kWcm}^{-2}$. Figure 4a demonstrates that the surface morphology is characterized by a random fluctuating dendritic feature. These features are in turn defined by the dentrite



(a)

200 μm



(b)

200 μm

FIGURE 4 Scanning electron micrographs of Ti6Al4V surface morphology at (a) $F = 90 \text{ Jcm}^{-2}$ and (b) $F = 210 \text{ Jcm}^{-2}$.

tip radius and their spacing (15–20 μm). It is, however, important to notice from a metallurgical point of view that melting initially begins from possible inclusions scattered at the surface due to a high temperature rise and gradual joining of these molten centers, producing a molten pool (Figure 4b).

Zone III begins with the thermal ablation of Ti6Al4V at $\geq 145 \text{ Jcm}^{-2}$. However, the plasma formation took place slowly at higher fluences and became more intense as this parameter was increased. Some cracks were observed at the laser-treated sites, which are believed to be due to residual mechanical stress originating from the temperature gradient at the end of the pulse. Also, other factors such as surface composition, degree of solubility of the alloys and base metal, thermal diffusion, and heating/cooling rate may have specific roles in crack formation, which need separate attention and analysis. Generally, because in our experiment the pulse duration is much greater than the thermal relaxation time (*i.e.*, $\tau_p \approx 200 \mu\text{s} \gg \tau_r \approx \alpha^{-2}/4k \approx 140 \text{ ns}$) and the optical absorption depth, α^{-1} , is much smaller than the thermal diffusion depth, z_t , (*i.e.*, $\alpha^{-1} \approx 2 \mu\text{m} \ll 2(k\tau_p)^{0.5} \approx 7.5 \text{ mm}$). The relation between surface temperature at the end of laser pulse and laser fluence can be shown as Equation (3), indicating a nonadiabatic condition,

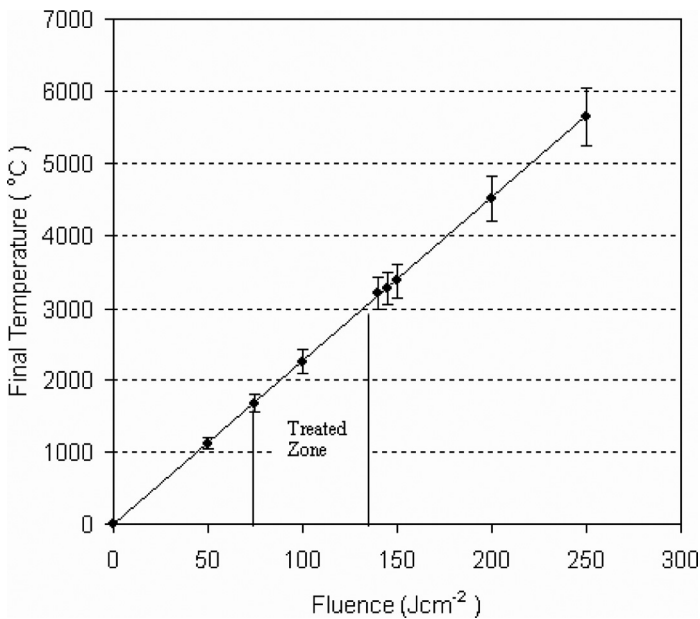
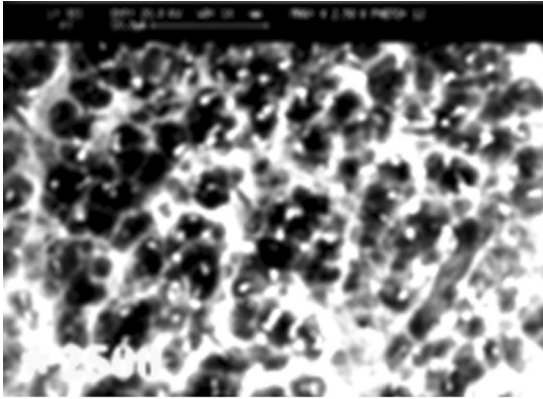


FIGURE 5 Variation of surface temperature *versus* laser fluence.

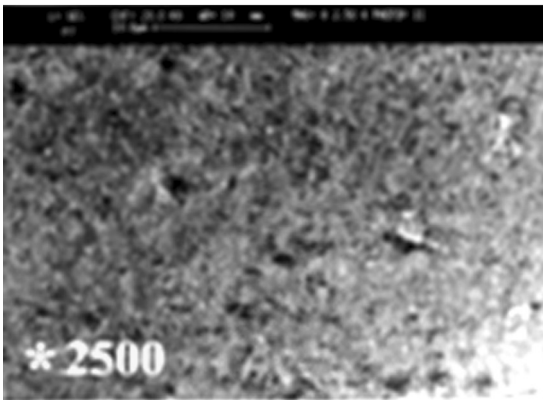
governing the experiment:

$$T_f - T_i = \frac{(1 - R)F}{\rho c(4k\tau_p)^{0.5}}, \quad (3)$$

where [19] T_f , T_i are final and initial surface temperature ($^{\circ}\text{C}$), R is surface reflection (0.6), C is specific heat capacity ($0.52 \text{ Jg}^{-1}\text{C}^{-1}$),



(a)



(b)

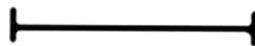

20 μm

FIGURE 6 Scanning electron micrographs of Ti6Al4V surface morphology (a) control and (b) laser treated at 140 Jcm^{-2} .

ρ is density (4.51 gcm^{-3}), k = diffusivity coefficient ($0.07 \text{ cm}^2\text{s}^{-1}$), and τ_p is pulse width ($200 \text{ }\mu\text{s}$).

Figure 5 indicates the variation of Ti6Al4V surface temperature as a function of laser fluence.

Now, by considering the melting and vaporization point of Ti6Al4V as 1668°C and 3280°C , respectively, and the threshold fluence of ablation as about 70 Jcm^{-2} using Figure 1, then it would be sensible to choose zone II as the treatment region (*i.e.*, below ablation).

The comparison between two morphologically different areas [*i.e.*, laser-treated and the control specimens (Figure 6)] indicates that the inclusion have disappeared and that the scratches due to machining and polishing are sealed with direct laser surface heating. Ti6Al4V alloy is a ($\alpha + \beta$) two-phase alloy with around 6 wt% aluminum stabilizing the α phase and about 4 wt% vanadium stabilizing the β phase. At room temperature, the microstructure at equilibrium consists mainly of primary α phase (hcp) with some retained β phase (bcc). It is also well known that in laser surface melting, the steep temperature gradient and thermal cycle lead to some microstructural changes in the heat-affected zone within a very short time. In particular, the $\alpha \rightarrow \beta$ phase transformation during rapid heating and decomposition of the β phase during rapid cooling needs to be considered. The physical and mechanical properties of Ti6Al4V alloy are known to be sensitive to its microstructure. The Ti- β phase, has a diffusivity two orders of magnitude higher than in the Ti- α phase, so the flow stress is strongly influenced by the ratio of the two phases present.

Surface Wettability

The change in surface wettability was studied by contact-angle measurement for all specimens treated at 100 Jcm^{-2} and 140 Jcm^{-2} (Figure 7).

A smoother surface was achieved by laser radiation at 140 Jcm^{-2} , which may affect the degree of wettability. It is, however, important to note that enhanced oxygen content, which depends on oxide layer thickness, can help to reduce the contact angle. This is because the surfaces with higher concentration of oxygen atoms and more incorporation of oxygen-based polar functionalities in the surface exhibit higher wettability (*i.e.*, lower contact angle), hence an improvement of biocompatibility, though some believe that hydrophilicity alone is an inadequate promoter of cell adhesion and retention [20]. As a result, better cell adhesion can be obtained for the specimens with apparently higher surface energy, rather than with higher surface roughness.

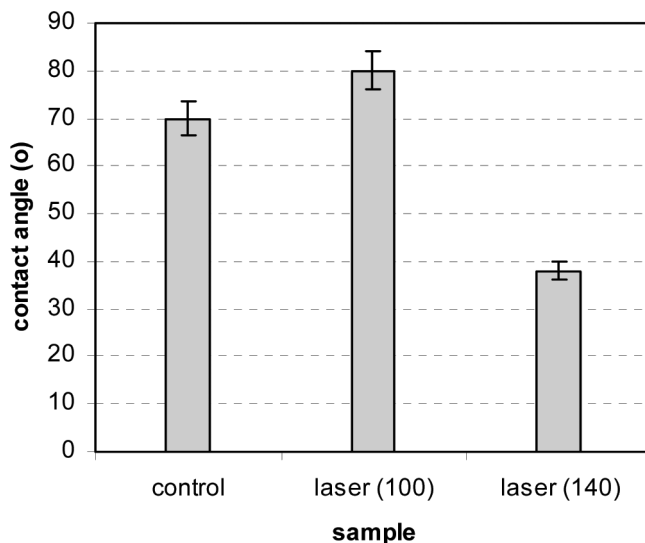


FIGURE 7 Contact angle measurement for different samples.

According to the topography of the primary melting centers, the surface roughness was increased slightly at 100 Jcm^{-2} . However, an increase of contact angle occurs from 70° to 80° , indicating a lower degree of wettability. Following the laser treatment at 140 Jcm^{-2} , the contact angle reduced to 37° , giving a more acceptable hydrophilicity.

Also, variation of surface tension for all specimens was calculated by measured contact angle. It is known that as contact angle decreases, the related surface tension will be increased. Therefore, a value of 58 mN/m was obtained for γ at 140 Jcm^{-2} , which is considerably higher than 39 mN/m of the control sample. The corresponding value of γ for 100 Jcm^{-2} , was found to be 32 mN/m (Figure 8).

Cell Culture

Figure 9 clearly illustrates the morphology and spreading of cells on the plate sample. Some of the attached cells spread radially from the center and developed filopodia (point a). The surface of cells not yet spread were convoluted into microridges (point b). Neighboring cells maintain physical contact with one another through multiple extensions (point c). Cell spreading is an essential function of cells adhered to any surface and precedes the function of cell proliferation to eventually provide a cell-covered surface.

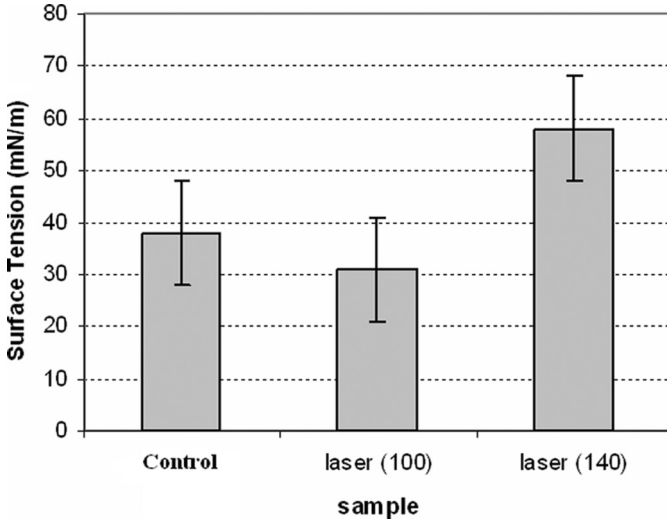


FIGURE 8 Variation of surface tension with surface texture.

Cell Spreading Analysis

The experimental results of bone cell growth are given in Table 1. As can be seen, cells spreading over the specimen surface relate to laser fluence and surface texture, which were measured by the Image J program software (IJP).

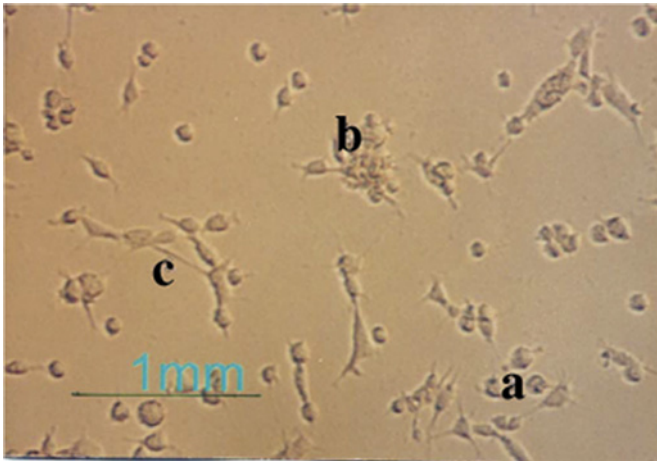


FIGURE 9 Spreading patterns of attached fibroblast cells on titanium plate.

TABLE 1 Spread of Bone Cells over the Implanted Specimen Surface (Average of 10 Measurements at 3 Separate Regions)

Row	Specimens	Spread cell area (μm^2)
1	control	316 ± 10
2	$F = 100 \text{ (Jcm}^{-2}\text{)}$	352 ± 6
3	$F = 140 \text{ (Jcm}^{-2}\text{)}$	488 ± 8

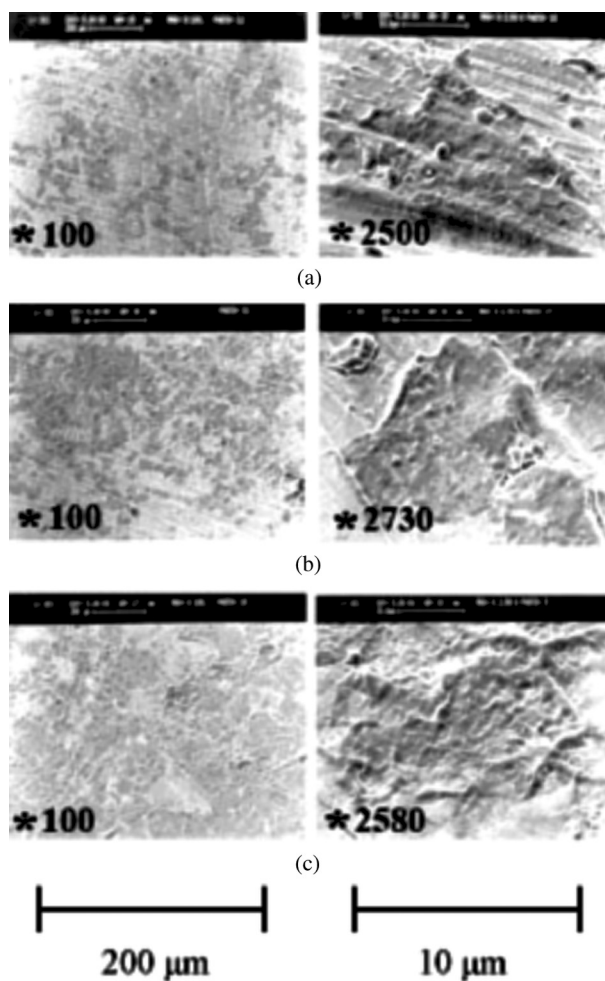


FIGURE 10 Scanning electron micrographs of attached cells on the surface for (a) control, (b) treated at 100 Jcm^{-2} , and (c) treated at 140 Jcm^{-2} .

The SEM analysis of the morphology of the attached cells (Figure 10) indicates that the density of the cell network is directly dependent on the laser beam fluence and surface topography. The smooth surface at 140 Jcm^{-2} not only caused a dense cell network but also resulted in a wider area covered by a single cell spreading. Density of the network originates from the change of monolayer attachment (cell–surface) multilayer (cell–surface and cell–cell). As is seen, no specific directional spread of attached cells was achieved in laser-treated specimens.

Evaluation of the number of cells attached to the implant surface as a function of time was done by an enzyme detachment test. Figure 11 clearly indicates that more cells are attached to the surface treated (1.2×10^5) at 140 Jcm^{-2} than are for the surface treated at 100 Jcm^{-2} (0.7×10^5) and for the control value of 0.4×10^5 .

Histopathological Evaluation

When the implants were retrieved, no inflammatory reaction was observed inside or around the implants. Mineralized matrix deposition and bone cells were observed on the surface of implants, which are formed

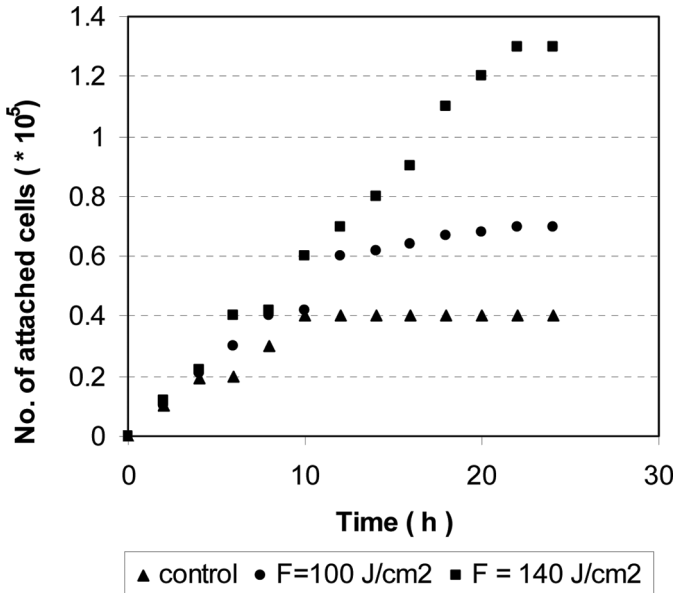


FIGURE 11 Number of attached cells on the surface of sample as a function of time.

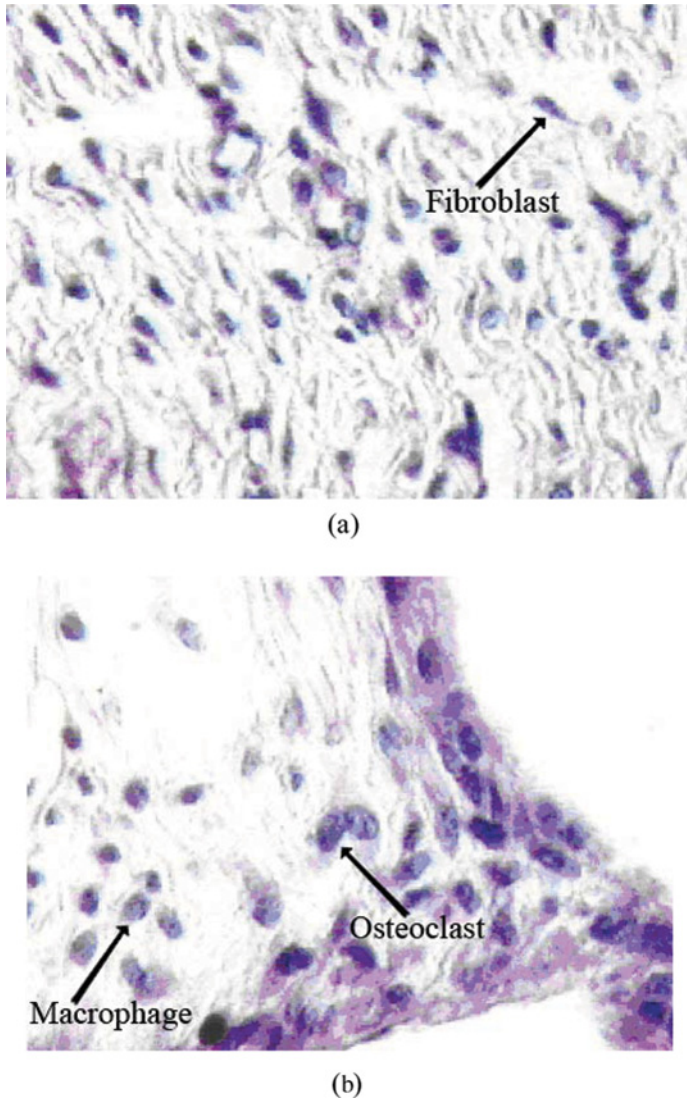


FIGURE 12 Light microscopy evaluation of the bone tissue for (a) laser treated at 140Jcm^{-2} and (b) control.

during the 8-month implantation (see Figure 2a). Mineralized matrix deposition was found on all sides of implants, and bone formation was characterized by the occurrence of osteocytes embedded in a mineralized matrix (Figure 12).

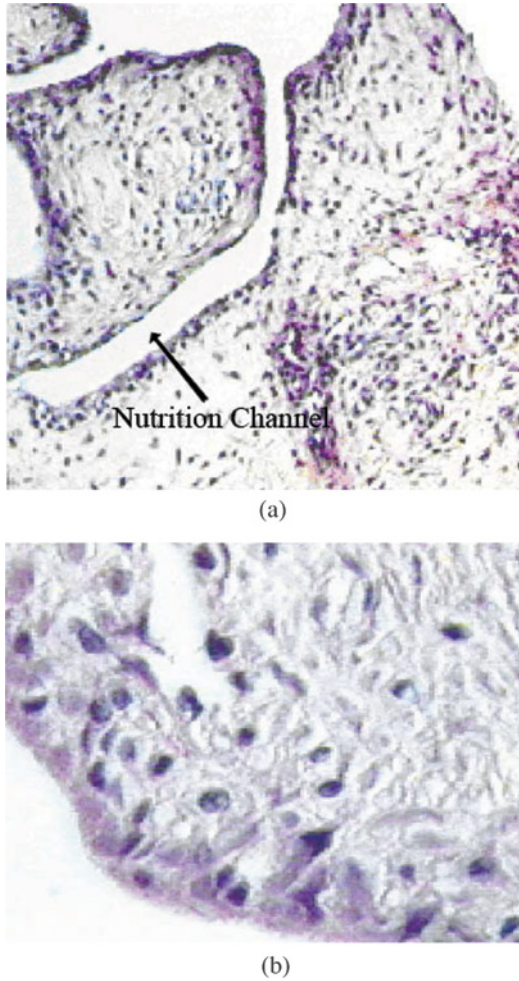


FIGURE 13 Light microscopy evaluation of bone tissue for (a) laser treated at 140 Jcm^{-2} with a nutrition channel shown and (b) control sample without the channel.

As is seen from Figure 13, the bone tissue nutrition is carried out through the channel around the laser treated sample whereas it was not observed in the case of the control sample.

Qualitative evaluation of macrophage, osteoblast, osteoclast, polymorphonuclear leukocytes (PMN), giant cells, fibroblast, lymphocyte, and healing was carried out during pathology tests (Table 2). The

TABLE 2 Qualitative evaluation of Histology Results of Bone Tissue Around the Implants with Different Surface Morphology

Sample Cell	100 Jcm ⁻²	140 Jcm ⁻²	Control
Fibroblast	+++	+++	++
Osteoblast	++	+++	+
Giant cell	-	-	-
Osteoclast	-	-	+
PMN	+	-	+
Lymphocyte	+++	++	++
Macrophage	+++	++	++
Healing	+	++	+

symbols given in Table 2 indicate the presence of 2-3 cells (+), 3-5 cells (++), more than 5 cells (+++), and lack of cells (-), respectively.

No PMN, giant cells, and osteoclasts were seen in the laser-treated sample at 140 Jcm⁻². Also tissue healing was better conducted near the mentioned implant rather than at all the other evaluated specimens. Fibroblast and osteoblast cells were also numerous on the qualitative scale for the 140 Jcm⁻² case.

DISCUSSION

The successful incorporation of bone implants strongly depends on a firm, long-standing adhesion of the tissue surrounding the implants. The cellular reaction is influenced by the properties of the bulk materials as well as the chemical composition and the topography of the surface [21-26]. When considering materials for application of orthopaedic implants, it is important to consider a number of factors such as biocompatibility and surface wettability.

However, because laser surface processing of materials is an area of considerable importance, technological parameters of radiation must be carefully optimized to obtain a desirable surface structure. The modification efficiency depends on the surface quality, the laser fluence, and the spatial and temporal profile of laser beam. The laser energy deposition, melting, and evaporation of titanium during the interaction process were shown to be dependent on the laser fluence, number of pulses, and pulse duration as well as on physical-chemical and optical properties of the material.

In the present study, laser-material interaction is considered as a nonadiabatic thermal process, with thermal evaporation as the dominant

mechanism. Therefore, selecting a correct energy density for surface treatment has a direct influence on surface wettability of Ti6Al4V. According to this study, surface laser treatment at 140 Jcm^{-2} produced a more acceptable effect on surface properties and cell adhesion.

In terms of biocompatibility, decrease of contact angle due to the surface treatment process can cause more cell adhesion to the surface, which subsequently can result in better biocompatibility. According to our results, two regions in Figure 1 are worth discussing. First, from 0 to 100 Jcm^{-2} , where the measured surface contact angle was increased with the surface roughness because of appearance of surface melting. Second, from 100 Jcm^{-2} to 140 Jcm^{-2} where the contact angle was decreased by about 50% when the surface became smoother.

In addition to surface morphology, the properties of implant materials affect cellular behavior such as wettability. The wettability of the surface plays an important role with respect to protein adsorption, cell attachment, and spreading. It is known that surfaces with high surface free energy are more adhesive than those with a low surface free energy. The surface tension at 140 Jcm^{-2} was about 1.5 times greater than the control sample. It is also worth noticing that all the samples were treated in ambient conditions and were steam sterilized, which would have a great influence on the surface composition of Ti, especially TiO_2 formation. It is proved that the samples irradiated by laser during treatment can lead to oxygen diffusion through the molten materials and thus to oxidation of titanium [24]. Also, the variation of surface oxidation layer thickness depends on the steam sterilization process and the time of exposure to air [25]. As was mentioned earlier, an increase in surface oxygen content depends on the growth of oxide layer thickness, which can lower the contact angle. If cells are affected by the presence of hydroxides on the surface, then developing an understanding of the mechanisms that control this interaction could lead to the optimization of this parameter in current and future metallic biomaterials [25,26]. It is also understood that no toxicity appeared after laser treatment considering *in vitro* analysis.

Bone cell adhesion to a surface depends directly on how easy the collagen or noncollagen proteins reach the surface, because they play an important role in the adhesion process. The focal point in the laser-treated surface at 140 Jcm^{-2} is approximately 10 nm, which is convenient for bone cells to get close, be activated, and attach to the surface to form an extracellular matrix (ECM). In this state, bone cells will spread over the smooth surface much more easily and fluently. It seems, however, that the laser-treated surface did not regulate the cell's shape in a manner similar to that in other investigations [17,18].

The first important step in surface bone formation is the amount of cells that are capable of attaching to the surface. Following this step, the other cells in the next layer attach move easily to the implanted specimen. Therefore, at 140 Jcm^{-2} more cell attachment to the surface takes place and hence a dense and multilayered adhesion sites are formed.

CONCLUSION

This investigation was focused on studying the topographical effects produced by laser radiation on goat bone cell adhesivity to Ti6Al4V implants. It is concluded from *in vitro* and preliminary *in vivo* tests that a Nd:YAG laser can induce a desirable surface modification on Ti6Al4V alloy if the physical and optical parameters are carefully optimized. The SEM and contact-angle measurements, together with *in vivo* experiments and histopathological evaluation, all confirm that a noble and biocompatible Ti alloy with better physical-chemical properties can be obtained for biomedical applications. Finally, we believe that more investigations are needed to further clarify the fundamentals of the adhesivity of cells on smooth surfaces and attachment rough surfaces.

REFERENCES

- [1] Ducheyne, P. and El-Ghannam, A., *J. Cell Biochem.* **56**, 162–167 (1994).
- [2] Vercaigne, S., Wolk, J., and Jansen, J., *Biomater.* **19**, 1093–1099 (1998).
- [3] Feng, B., Weng, J., and Yang, B., *Biomater.* **24**, 4663–4670 (2003).
- [4] Brems, H. J. and Helsen, J. A., *Metals as Biomaterials* (Wiley: West Sussex, UK, 1998), pp. 30–70.
- [5] Wrentz, J. R., Lane, J. M., and Burstein, R., *J. Orthopaed. Res.* **14**, 85–93 (1996).
- [6] Anselme, K., *Biomater.* **21**, 667–681 (2000).
- [7] Thomas, C. H., McFarland, C. D., Jenkins, M. L., and Reznia, A., *J. Biomed. Mater. Res.* **37**, 81–93 (1997).
- [8] Cooper, L. F., Masuda, T., Yliheikkilä, P. K., and Felton, D. A., *Int. J. Oral Maxillofac. Implants.* **13**, 163–174 (1998).
- [9] Davies, J. E., *Anat. Rec.* **245**, 426–445 (1996).
- [10] Masuda, T., Yliheikkilä, P. K., Felton, D. A., and Cooper, L. F., *Int. J. Oral Maxillofac. Implants.* **13**, 17–29 (1998).
- [11] Meyer, U., Szulezewski, D. H., Moller, K., Heide, K., and Jones, D. B., *Cells Mater.* **3**, 129–140 (1993).
- [12] Peyer, P., Scherpereel, X., Berthe, L., Carboni, C., Fabbro, R., and Lemaitre, C., *Mat. Sci. Eng.* **280**, 294–302 (2000).
- [13] Tritca, S., Gakovic, M., Nenadovic, M., and Mitrovic, M., *Appl. Sur. Sci.* **177**, 48–57 (2001).
- [14] Beraceras, I., Alava, I., Onate, J. I., and Maezto, M. A., *Surf. Coat. Technol.* **28** (36), 158–159 (2002).

- [15] Tritca, M. S., Tarasenko, V., Gakovic, B., and Fedenev, A., *Appl. Sur. Sci.* **252**, 474–482 (2005).
- [16] Hollander, D., Walter, M., Wirtz, T., Paar, O., and Eril, H., *Biomat.* **27**, 955–963 (2005).
- [17] Hao, L., Lawrence, J., and Li, L., *Appl. Sur. Sci.* **247**, 453–457 (2005).
- [18] Hao, L., Lawrence, J., and Li, L., *Appl. Sur. Sci.* **247**, 602–606 (2005).
- [19] Ifflander, R., *Solid State Lasers for Material Processing* (Springer, Schramberg, Germany, 2001), chap. 3., pp. 257–328.
- [20] Baier, R. E., Meyer, A. E., Natiella, J. R., Natiella, R. R., and Carter, J. M., *J. Biomed. Mater. Res.* **18**, 337–355 (1984).
- [21] Birte, G. S., Neubert, A., Hopp, M., Griepentrog, M., and Lange, K. P., *J. Biomed. Mater. Res.* **64A**, 591–599 (2003).
- [22] Sikavitsas, V. I., Dolder, J., Bancroft, G., and Jansen, J., *J. Biomed. Mater. Res.* **67A**, 944–951 (2003).
- [23] Fischer, P., Leber, H., Romano, V., Webber, H. P., and Glardon, R., *Appl. Phy. A* **A78**, 1219–1227 (2004).
- [24] Ronold, H. J., Lyngstadaas, S. P., and Ellingsen, J. E., *J. Biomed. Mater. Res.* **67A**, 524–530 (2003).
- [25] Peto, G., Karacs, A., Paszti, Z., Guzzi, L., Diviny, T., and Joob, A., *Appl. Surf. Sci.* **186**, 7–13 (2002).
- [26] Gyorgy, E., Mihailescu, I. N., Serra, P., and Morenza, J. L., *Surf. Coating Tech.* **154**, 63–67 (2002).